Hydrogen Embrittlement Susceptibility of Corrosion-Resistant Spring Rod Used in High-Speed Railway

Jinbo Li [1,2], **Xiuhua Gao** [1,*], **Hongwei Chen** [3], **Hongyan Wu** [1], **Linxiu Du** [1] **and Chen Chen** [1]

1   State Key Laboratory of Rolling and Automation, Northeastern University, Shenyang 110819, China
2   HBIS Group Hansteel Company, Handan 056015, China
3   HBIS Group Technology Research Institute, Shijiazhuang 050023, China
*   Correspondence: gaoxiuhua@126.com; Tel.:+86-024-83670360

Abstract: The corrosion of spring steel is very important for vehicle safety. In this work, we conducted an experiment on multi-element micro-alloy composition design; the corrosion resistance of a 60Si2Mn spring was improved by adding Cr, Ni, Cu and other corrosion-resistant elements, and the corrosion resistance index (I) was increased from 3.21 to 8.62. Hydrogen embrittlement resistance was studied using a hydrogen permeation experiment and a slow strain rate tensile experiment. For this study, the following steps were performed: Firstly, the material composition was designed, and the experimental materials that met the experimental design were prepared according to the corresponding deformation and heat treatment process; secondly, the experimental materials were charged with hydrogen; and finally, conventional tensile testing, slow tensile testing and fracture morphology testing were carried out. A hydrogen permeation experiment was carried out for the materials. The result showed that, with the increase of hydrogen charging time, the hydrogen content of two steel samples increased, and the plasticity indexes such as elongation and reduction of the area appeared in three different stages which rapidly decreased, slowly declined, and then tended to balance. The uniform NbC nano precipitated phase can double the number of irreversible hydrogen traps (Nir) per unit volume, and decreased the effective hydrogen diffusion coefficient (Deff) from 1.135×10^{-10} to 6.036×10^{-11}. It limited the free diffusion of hydrogen and made the immersed hydrogen harmless, thus improving the hydrogen embrittlement resistance of corrosion-resistant spring steel 60Si2Mn.

Keywords: hydrogen embrittlement; spring steel; high-speed rail elastic strip; hydrogen permeation; hydrogen trap

1. Introduction

With the development of China's high-speed railway, the demand for spring steel for high-speed rail has increased rapidly [1]. The spring rod is the most important part of a railway track fastener, which mainly uses the energy stored during elastic deformation to reduce vibration and impact. Due to the fast running speed of a high-speed railway, the amplitude and load of spring rods are greater than those of ordinary lines, and the high-speed railway is sensitive to small defects and pits [2,3].

The surface of a spring rod for a high-speed railway is coated with a layer of coating to improve the corrosion resistance before installation [4–7]. In recent years, it was found that, with the extension of service time, the corrosion of spring rods in railway fasteners became increasingly serious, and their performance was seriously affected. There was a risk of failure and fracture, which greatly threatened the service life of spring rods. Therefore, it is very important to develop spring steel that not only has the mechanical properties of a spring rod for high-speed railway but also has excellent corrosion resistance [8,9].

As the tensile strength of spring steel is becoming higher and higher, the problem of hydrogen embrittlement caused by high strengthening is becoming more prominent [10,11].

On the one hand, hydrogen comes from the hydrogen in the spring steel manufacturing process [12]. On the other hand, in the actual service process, hydrogen atoms are generated on the steel's surface due to the cathodic corrosion reaction [13], which causes the increase of the hydrogen concentration in the steel solution. When the concentration of hydrogen atoms reaches a certain threshold, the crack initiation process accelerates the propagation and, finally, hydrogen embrittlement failure and instant fracture occur [14,15]. There are many types of research on the hydrogen embrittlement mechanism [16,17], including hydrogen pressure theory, dislocation interaction theory, hydrogen reducing surface energy theory, and hydrogen induced local plastic deformation theory, etc. [18]. The factors affecting hydrogen embrittlement sensitivity include the strength, microstructure, and hydrogen trap of steel. Domestic research mainly focuses on martensitic steel, dual-phase steel, and transformation-induced plasticity steel [19,20], while research on spring steel is rare. Especially in recent years, the spring rods for high-speed rail have been widely used [21]. It is of great significance to ensure the hydrogen embrittlement resistance of spring steel [22,23] and develop spring steel with good corrosion resistance and hydrogen embrittlement resistance [24,25].

Masoud Moshtaghi and Tomoki Doshida [26,27] et al. have conducted relevant research to investigate the joint effect of temperature and strain rate on the hydrogen embrittlement properties of martensitic steel. At 50 °C, the elongation loss first increases and then decreases with a decrease of the strain rate. It was first reported that, at the low strain rates, hydrogen embrittlement susceptibility was mitigated by temperature due to an increase in the hydrogen effusion to the surface of the material and the release of a significant amount of hydrogen before the yield point due to the temperature effect. At 25 °C, elongation loss increases with decreasing strain rate, since at the lower strain rates, the hydrogen can interact with mobile dislocations, which finally leads to H-induced fracture. The specimen fractured under elastic stress in the presence of hydrogen showed, macroscopically, a brittle fracture without necking. The fractured surface was attributed to localized plastic deformation, since the morphology of the microscopic fracture surface was mostly a quasi-cleavage fracture. The increased lattice defects in the near-fracture area were subsequently removed by annealing at 200 °C. The mean positron annihilation lifetime measured with the PPMA for a fractured specimen was longer in the near-fracture area than in other areas. Thus, the most probable reason for the increase in the amount of lattice defects can be ascribed to an increase in the amount of vacancies or vacancy clusters. Regarding hydrogen embrittlement involving microscopic plastic deformation, the localized enhanced vacancies due to interactions between dislocations and hydrogen under elastic stress directly caused ductility loss, because ductility loss occurred even though hydrogen was completely removed by degassing before the tensile test. Besides hydrogen content and applied stress, the time of formation and the accumulation of vacancies are also concluded to be important factors causing hydrogen embrittlement. There is no report on the application of the above research results to the railway spring rod.

In this paper, through the rolling and heat treatment process, the composition and content of a multi-element micro-alloy were designed to precipitate the NbC nanophase, which can double the number of irreversible hydrogen traps (Nir) per unit volume based on meeting the service conditions of corrosion-resistant spring steel. The hydrogen evenly distributed in the grain can inhibit the hydrogen embrittlement of high-strength spring steel and solve the problem of hydrogen embrittlement and hydrogen damage of high-strength spring steel under the condition of ensuring corrosion resistance. It has important theoretical value for developing and perfecting the research on hydrogen embrittlement resistance.

2. Materials and Methods

The experimental sample materials were corrosion-resistant 60Si2Mn NH spring steel (referred to as material A) and conventional 60Si2Mn spring steel (referred to as material B). Their chemical compositions are listed in Table 1. Based on material B, the atmospheric corrosion of material A was improved by adding elements such as Cu, Ni, and Cr, which

can improve the corrosion resistance of the material. The trace Nb was added, forming the second phase of NbC to refine the grains. The relevant samples were prepared by hot rolling and heat treatment. The heat treatment process of material A was at 960 °C for 0.5 h, 847–860 °C for oil quenching, 485 °C for tempering, and 1.5 h for holding. The heat treatment process of material B was at 960 °C for 0.5 h, 860–880 °C for oil quenching, 440 °C for tempering and 1.5 h for holding. The hydrogen brittleness resistance was studied using a slow strain rate tensile test and a hydrogen permeation test. The hydrogen embrittlement resistance of the experimental steel was evaluated according to the change of mechanical properties before and after hydrogen charging, the effective hydrogen diffusion coefficient, and the number of hydrogen traps per unit volume during hydrogen permeation.

Table 1. Chemical composition of spring steel (Mass Fraction, %).

Material	C	S	Si	Mn	P	Cr	Ni	Cu	Nb
Material A	0.60–0.63	0.020	1.50–1.7	0.80–1.00	$\leq$0.025	0.20–0.35	0.20–0.30	0.25–0.30	0.02–0.03
Material B	0.60–0.63	$\leq$0.020	1.50–1.7	0.80–1.00	$\leq$0.025	-	-	-	-

2.1. Electrolytic Hydrogen Charging

The electrolytic hydrogen charging experimental device is a single electrolytic cell structure. A 1000 mL beaker was used as the electrolytic cell. Six graphite electrodes were symmetrically placed inside the beaker. The sample was placed in the center of the beaker and connected to the negative pole of the IDX IT6720 digital display DC stabilized voltage power supply (ITECH Electronics Co. Ltd., Tokyo, Japan). The sample was used as the cathode, and the graphite electrode was used as the anode. The graphite electrode was connected to the positive pole of the power supply. Then, 5% H_2SO_4 aqueous solution was taken with 0.3 g/L thiourea as an electrolyte solution, the hydrogen charging current was 15 mA, and the hydrogen charging times were 0.5 h, 1 h, 1.5 h, and 2 h.

2.2. Mechanical Property Test

The mechanical properties were tested using a conventional tensile test and a slow strain rate tensile test. The slow strain rate tensile test was carried out on a Shimadzu AG-X universal test machine, and the gauge length of the tensile specimen was 50 mm. The tensile rate used in a conventional tensile test is 3 mm/min, and the tensile rate used in a slow strain rate tensile test is 0.1 mm/min. Figure 1 shows the sample size of the slow strain rate tensile test.
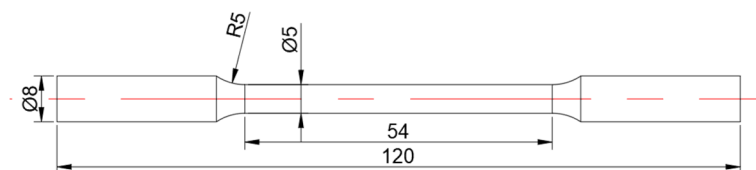
Figure 1. Slow strain rate tensile test specimen (/mm).

2.3. Hydrogen Permeation Test

A Devanathan Stachurski double electrolytic cell hydrogen permeation testing device (Fe-HP-12 metal hydrogen permeability tester, Northeastern University, Shenyang, China) As shown in Figure 2, was used for the hydrogen permeation experiment. The hydrogen permeation test process was conducted according to standard ISO17081-2014. In the experiment, the solution of the hydrogen charging pool was a 0.2 mol/L NaOH solution + 17 mol/L saturated Na_2S solution, and the solution of the hydrogen releasing pool was a 0.2 mol/L NaOH solution. The hydrogen permeation sample was an 80 mm (RD) × 50 mm (TD) × 1 mm (ND) sheet steel. Before the experiment, the samples were electropolished and anodized. The mass fraction of each component in the electropolishing solution was 70% H_3PO_4 + 10% H_2SO_4 + 9% CrO_3 + 11% H_2O, while the mass fraction of

the anodized solution was 10% diluted hydrochloric acid. Then, one side of the sample was plated with nickel. The mass ratio of each chemical in the plating solution used was m (H_2O):m ($NiSO_4 \cdot 7H_2O$):m ($NiCl_2 \cdot 6H_2O$):m (H_3BO_4) = 1000:125:22.5:20. During hydrogen permeation, a sample with a thickness of 1 mm was placed between the hydrogen charging pool and the hydrogen releasing pool, and the contact area between the sample and the solution on both sides was 7.065 cm^2 (30 mm in diameter). The nickel-plated surface of the sample was the anode side (hydrogen-releasing side), and the nickel-free surface was the cathode side (hydrogen-charging side). Nitrogen was continuously introduced into both electrolytic cells to remove oxygen. The anode side was plated with nickel to prevent the steel substrate from being oxidized, and the potentiostat parameters were set to make the sample at potentiostatic polarization with a constant potential of 250 mV. After the residual current at the anode side decreased to a stable state, the hydrogen charging current at the hydrogen charging side was set to 4 mA/cm^2 to promote hydrogen penetration into the steel. After the current at the anode side increased to a stable state, the first hydrogen charging process was completed. After that, the hydrogen charging current was set to zero, and the anode side current started to decrease. After the anode side current decreased to a stable state again, the second hydrogen charging was started. The hydrogen charging parameters were the same as those in the first experiment. After that, the curve of the anode side current changes with time could be obtained.
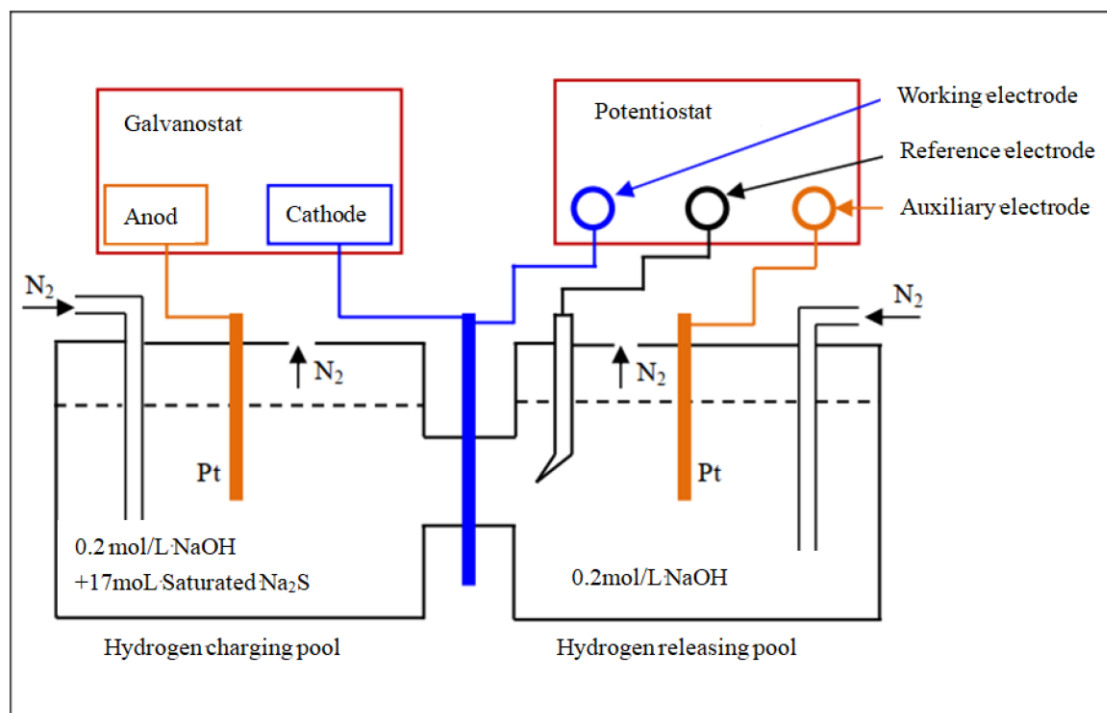
Figure 2. Schematic diagram of hydrogen permeation test device.

According to the ISO 17081-2014 standard, hydrogen permeation parameters such as hydrogen permeation flux (J_{ss}), effective hydrogen diffusion coefficient (D_{eff}), hydrogen concentration (C_0) on the hydrogen charging side of the sample, number of hydrogen traps per unit volume (N_T), and irreversible hydrogen traps per unit volume (N_{ir}) were calculated. The calculated formulas are shown in (1)~(6).

$$J_{ss} = \frac{i_{ss}}{AF} \tag{1}$$

$$D_{eff} = \frac{L^2}{6t_{lag}} \tag{2}$$

$$C_0 = \frac{J_{ss}L}{D_{eff}} \tag{3}$$

$$D_{eff} = D_L(1 + \frac{3N_T}{N_A.C_0})^{-1} \tag{4}$$

$$N_T = \frac{N_A.C_0}{3}(\frac{D_L}{D_{eff}} - 1) \tag{5}$$

$$N_{ir} = N_{T1} - N_{T2}, \tag{6}$$

where i_{ss} is the steady state current density of hydrogen permeation, A; A is the contact area between the sample and solution, m²; F is the Faraday constant, C/mol; L is the sample thickness, mm; t_{lag} is the time corresponding to $i/i_{ss} = 0.63$, s; i is the instantaneous current during hydrogen permeation; D_L is the diffusion coefficient of hydrogen in the lattice, 9.5×10^{-5} m²/s; N_A is the Avogadro constant, 6.022×10^{23}; and N_{T1} and N_{T2} are the number of hydrogen traps per unit volume measured during the first and second hydrogen permeations, respectively, m^{-3}.

3. Results and Discussion

3.1. Effect of Hydrogen on Mechanical Properties of Spring Steel

The value of I is an index related to the corrosion resistance of the material. The higher the value of I, the better the corrosion resistance of the material. According the to Legault–Leckie Formula (7) [28,29]:

$$I = 26.01(\%Cu) + 3.88(\%Ni) + 1.20(\%Cr) + 1.49(\%Si) + 17.28(\%P) - 7.29(\%Cu)(\%Ni) - 9.10(\%Ni)(\%P) - 33.39(\%Cu)^2. \tag{7}$$

The I values of three spring steel samples are calculated by the Formula (7): I_A (material A) = 8.62, I_B (material B) = 3.21. From the I value, the corrosion resistance of corrosion-resistant 60Si2Mn NH spring steel with added corrosion-resistant elements is much higher than that of the conventional 60Si2Mn spring steel.

Table 2 shows the results of the mechanical properties of the experimental steel after conventional tension. It can be seen from the table that the strength, elongation, and hardness of the two spring steel samples are similar, and the overall mechanical properties of the corrosion-resistant spring steel are slightly improved. Figures 3 and 4 show the comparison and change of the mechanical property indexes of two types of spring steel after a slow strain rate tensile test after hydrogen charging for 0.5 h, 1 h, 1.5 h, and 2 h. It can be seen from the figure that the two kinds of experimental steel show three stages of changes with the increasing hydrogen charging time, that is, the hydrogen content in the steel increases and the plasticity indexes, such as elongation and reduction of the area, show a rapid decline, a slow decline and then tend to balance. The change rules of elongation and reduction of area are consistent. The plasticity index decreases significantly after the hydrogen is never charged and 0.5 h after the hydrogen is charged, which reflects the damage hydrogen causes to the plasticity index. With the increase of hydrogen charging time, the hydrogen content in the steel increases until the hydrogen content of the steel reaches saturation, and the damage gradually reaches equilibrium.

Table 2. Conventional tensile mechanical properties after heat treatment.

Material	Yield Strength /MPa	Tensile Strength/MPa	Elongation $A_{11.3}$ /%	Reduction of Area/%	Hardness /HRC
Material A	1470	1594	6.0	30.1	46.9
Material B	1457	1572	5.2	30.6	45.3

At the same time, it can be seen that the plasticity index of corrosion-resistant spring steel A is better than that of conventional spring material B, and the reduction rate of the plasticity index caused by hydrogen damage is lower than that of conventional spring steel under the same hydrogen charging time. However, with the increase of hydrogen charging time, the gap between the reduction of elongation and the area reduction of the two experimental kinds of steel gradually decreases.
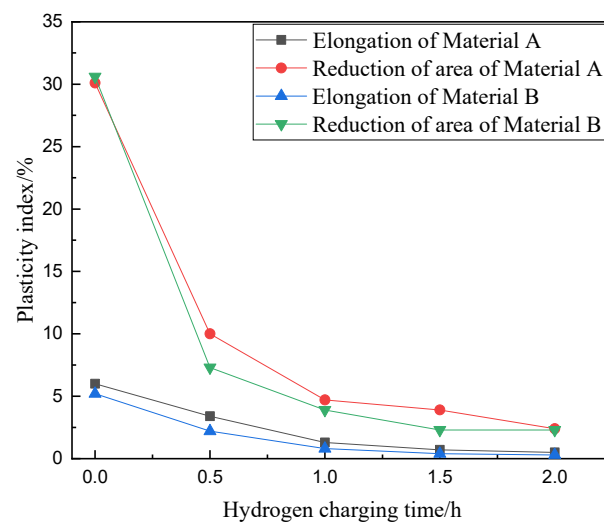
Figure 3. Plasticity index curve at different hydrogen charging times.
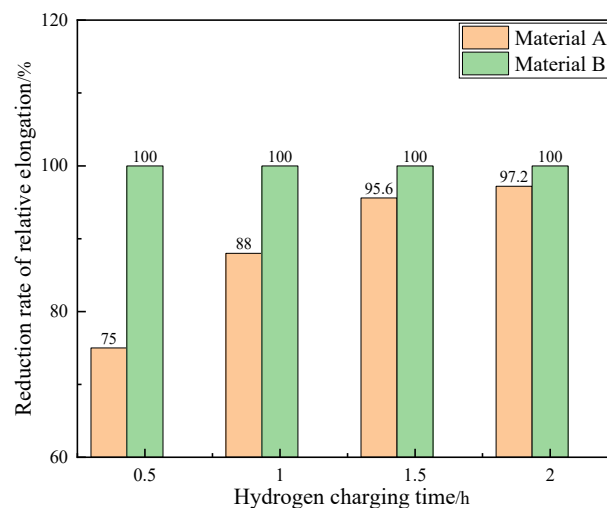
Figure 4. Relative elongation reduction rate at different hydrogen charging times.

3.2. Fracture Morphology Analysis

Figures 5 and 6 show the slow strain rate tensile fracture morphology of material B and material A. It can be seen that the normal strain rate tensile fracture surface of the two types of steel without hydrogen charging is dimple morphology. After hydrogen charging, the number of dimples decreases, and local quasi-cleavage morphology gradually appears. The proportion of quasi-cleavage morphology increases with the increase of hydrogen charging time. When the hydrogen charging time reaches 2 h, the area of quasi-cleavage morphology increases significantly. At the same hydrogen charging time, compared with material B, material A has more dimples and larger sizes of its fracture morphology. With the increase of hydrogen charging time, the area of quasi-cleavage morphology increases less.

3.3. Hydrogen Permeation Behavior

There are many hydrogen traps (such as precipitates, grain boundaries, dislocations, vacancies, etc.) in high-strength steel [30–32], and hydrogen atoms can be enriched on these traps [33]. Delayed fracture of high-strength steel is caused by room temperature diffusible hydrogen. However, diffusible hydrogen is not uniformly distributed in steel and it is affected by the nature, size, and distribution of reversible hydrogen traps [34]. The diffusion process of hydrogen in materials is affected by the existence of hydrogen traps [31]. One of the effective ways to improve the hydrogen embrittlement resistance of high-strength steel is to increase the number of hydrogen traps in steel by changing the chemical composition of the steel and using reasonable heat treatment process [35–37].
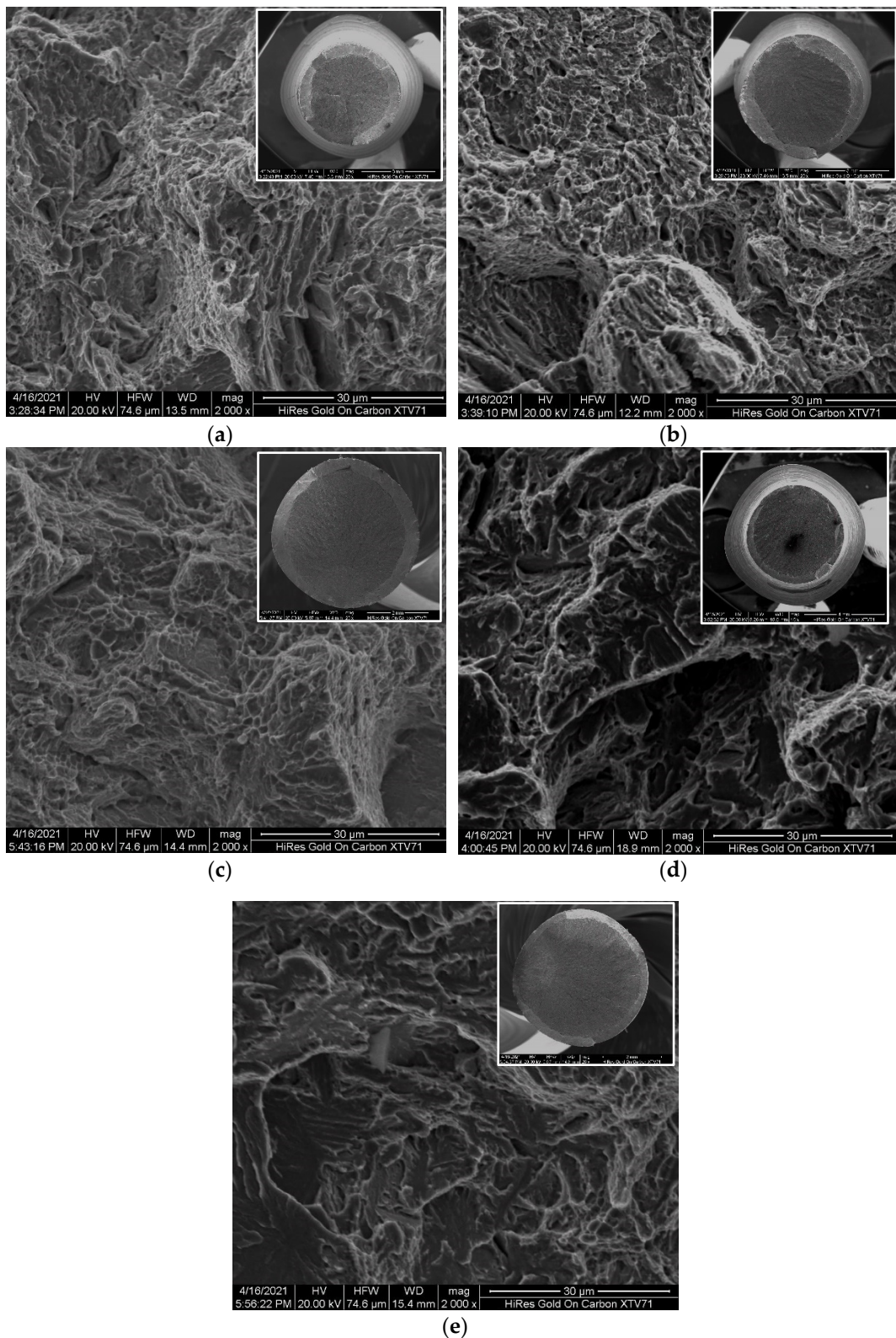
Figure 5. Tensile fracture morphology of material B. (**a**) Normal strain rate tensile test without hydrogen charging; (**b**) Hydrogen filling 0.5 h slow strain rate tensile test; (**c**) Hydrogen filling 1.0 h slow strain rate tensile test; (**d**) Hydrogen filling 1.5 h slow strain rate tensile test; (**e**) Hydrogen filling 2.0 h slow strain rate tensile test.
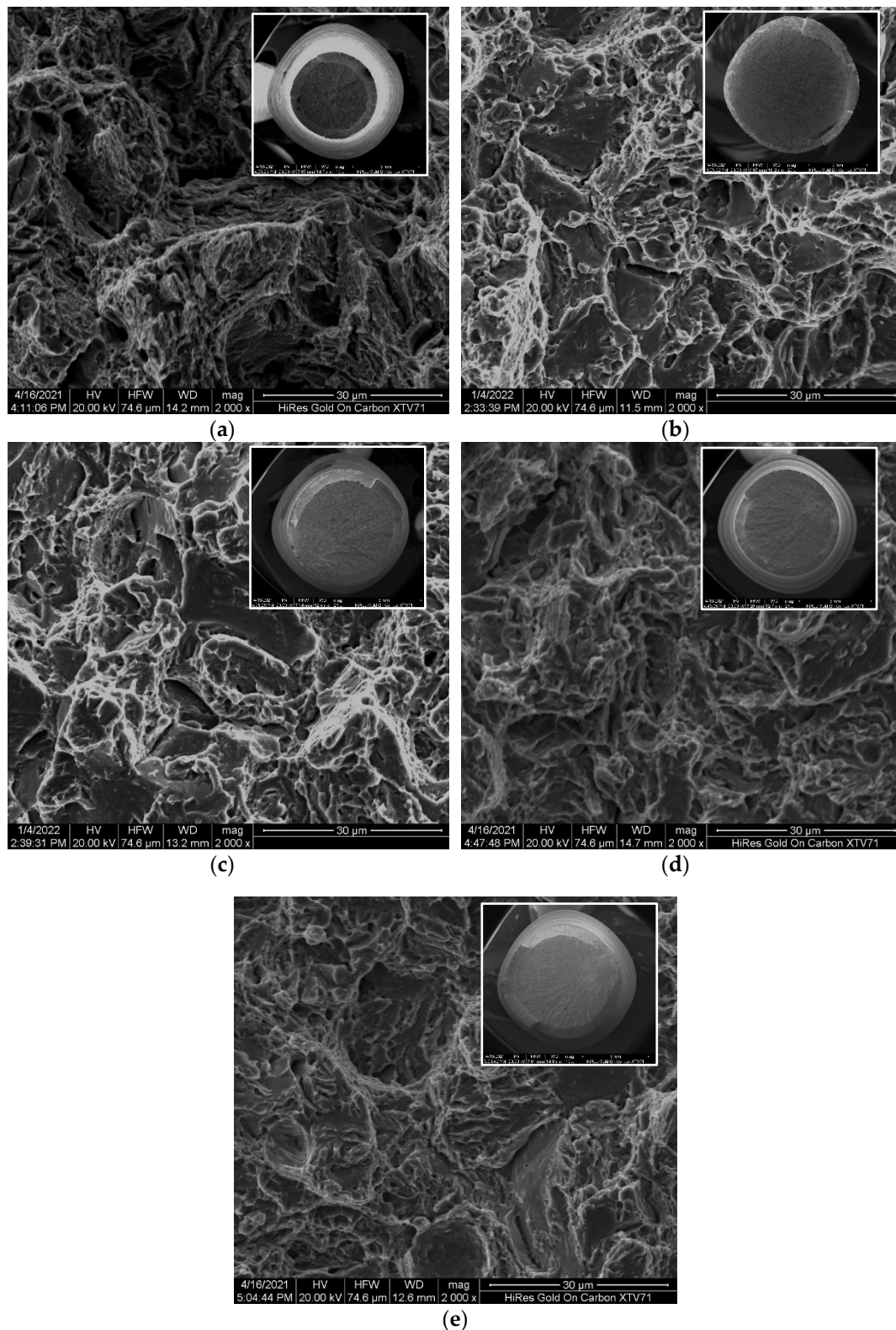
Figure 6. Tensile fracture morphology of material A. (**a**) Normal strain rate tensile test without hydrogen charging; (**b**) Hydrogen filling 0.5 h slow strain rate tensile test; (**c**) Hydrogen filling 1.0 h slow strain rate tensile test; (**d**) Hydrogen filling 1.5 h slow strain rate tensile test; (**e**) Hydrogen filling 2.0 h slow strain rate tensile test.

Hydrogen traps have a great impact on the solubility, diffusion, and enrichment of hydrogen. According to the binding energy of traps, hydrogen traps can be divided into reversible traps and

irreversible traps [38–41]. If the binding energy E of the hydrogen and the trap is large, hydrogen cannot escape from the trap and participate in diffusion at room temperature [42–44]. Such traps are irreversible traps. They can absorb hydrogen from their surroundings and prevent enough hydrogen from concentrating on the potentially dangerous parts that are prone to crack nucleation [45–50]. Therefore, controlling the type, quantity, and distribution of traps is one of the important ways to improve the delayed fracture resistance of materials [51–57].

Based on the research of Masoud Moshtaghi and Tomoki Doshida et al. [26,27], it can be inferred that fine carbides that are dispersed and precipitated are generated to refine grains. As a hydrogen trap with high binding energy, NbC is an irreversible hydrogen trap. A large number of particles are precipitated inside grains to effectively capture hydrogen, inhibit the diffusion of hydrogen, make hydrogen in steel evenly distributed, and make invading hydrogen harmless. Nb and C form NbC particles by adding trace elements of Nb. NbC precipitates in the grain boundary during tempering hinder the expansion of the grain boundary, which plays a role in refining the grain and improving the delayed fracture resistance. Figure 7 shows the hydrogen permeation curve of experimental steel under the same heat treatment process obtained after the hydrogen permeation experiment. In the first hydrogen permeation process, a large number of irreversible hydrogen traps in the steel have captured hydrogen, and the captured hydrogen cannot escape from the irreversible hydrogen traps position. Therefore, in the second hydrogen permeation process, only reversible hydrogen traps remain in the steel that can capture hydrogen, and the total number of hydrogen traps decreases significantly. Therefore, the second hydrogen permeation time is shorter than the first one.

(**a**)   (**b**)
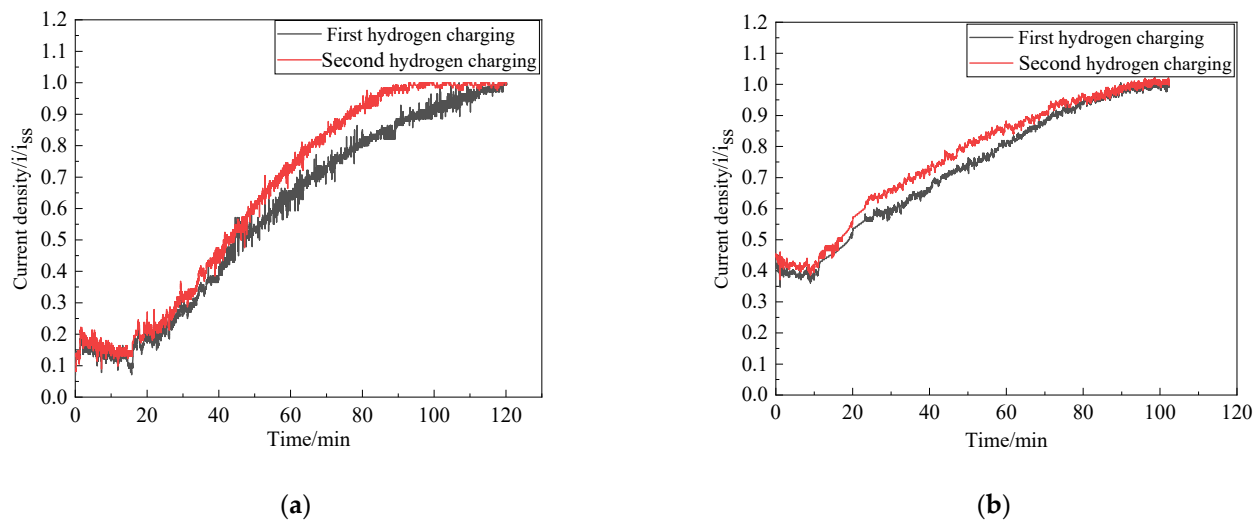
Figure 7. Variation of normalized current density with time. (**a**) Material A; (**b**) Material B.

The calculated results of the hydrogen diffusion parameters are shown in Table 3. It can be seen that the number of hydrogen traps per unit volume (N_T) and the number of irreversible hydrogen traps per unit volume (N_{ir}) in material A are significantly increased nearly one time compared with material B, and the effective hydrogen diffusion coefficient (D_{eff}) is significantly lower one time than material B. This is mainly due to the high binding energy of NbC in material A, which can be used as irreversible hydrogen traps to capture hydrogen in steel, and hydrogen cannot be diffused in steel. It reduces the amount of diffusible hydrogen in steel, so the invalidation of hydrogen penetrating steel greatly improves the hydrogen solubility and hydrogen embrittlement resistance.

Table 3. Calculation results of hydrogen diffusion parameters.

Material	D_{eff}/(m²·s⁻¹)		C_0/(mol·m⁻³)		N_T/m³		N_{ir}/m³
	First Hydrogen Charging	Second Hydrogen Charging	First Hydrogen Charging	Second Hydrogen Charging	First Hydrogen Charging	Second Hydrogen Charging	
Material B	8.146×10^{-11}	1.135×10^{-10}	3.88	2.61	9×10^{25}	4.33×10^{25}	4.67×10^{25}
Material A	4.681×10^{-11}	6.036×10^{-11}	4.39	3.29	1.78×10^{26}	9.29×10^{25}	8.51×10^{25}

Research shows that the development of high-strength martensitic steels can control the precipitation of C, N and other nano compounds by optimizing the composition design of micro alloys and matching reasonable heat treatment, and form a benign "hydrogen trap", thus reducing the risk of delayed cracking caused by hydrogen in the process of application. This paper compared the precipitation forms and hydrogen trapping sites of Ti, Nb and Cu alloy elements in martensitic steels under different heat treatment processes, and evaluated the hydrogen trapping ability of precipitated phases in high-strength martensitic steels. The results show that the hydrogen capture capacity is ranked as follows: NbC > TiC > grain boundary > e-Cu > dislocation, and the compound addition of microalloying elements can have a better anti-hydrogen embrittlement effect [58–60].

4. Conclusions

In this paper, the corrosion resistance of 60Si2Mn spring steel can be effectively improved by adding Cr, Ni, and Cu corrosion-resistant elements. the corrosion resistance of 60Si2Mn spring was improved by adding Cr, Ni, Cu and other corrosion-resistant elements, and the corrosion resistance index (I) has been increased from 3.21 to 8.62. With the Nb alloy element, the hydrogen embrittlement resistance of 60Si2Mn spring steel is enhanced. The following conclusions can be drawn:

(1) The mechanical properties of conventional 60Si2Mn spring steel and Niobium-containing corrosion-resistant 60Si2Mn spring steel decrease after hydrogen charging. The longer the hydrogen charging time, the greater the decline;

(2) The decreased rate of mechanical properties of Niobium-containing corrosion-resistant 60Si2Mn spring steel is lower than that of conventional 60Si2Mn spring steel with the same hydrogen charging time. The difference in this value gradually becomes smaller as the hydrogen charging time increases;

(3) Compared with the conventional 60Si2Mn spring steel, the number of hydrogen traps (N_T) per unit volume of Niobium-containing corrosion-resistant 60Si2Mn spring steel significantly increases, and the effective hydrogen diffusion coefficient (D_{eff}) significantly decreases. Using the uniform NbC nano precipitated phase as hydrogen traps can double the number of irreversible hydrogen traps (N_{ir}) per unit volume, and decreased the effective hydrogen diffusion coefficient (D_{eff}) from 1.135×10^{-10} to 6.036×10^{-11}. It limited the free diffusion of hydrogen and made the immersed hydrogen harmless, thus improving the hydrogen embrittlement resistance of corrosion-resistant spring steel 60Si2Mn.

Author Contributions: J.L. and X.G. conceived and designed the experiments; J.L. and C.C. performed the experiments; H.C. and H.W. analyzed the data; H.C. contributed the experimental material and analysis tools; L.D. supervised this paper; and J.L. and X.G. wrote the paper. All authors have read and agreed to the published version of the manuscript.

Funding: This research was funded by The National Key Research and Development Program of China (No. 2022YFB3706400).

Institutional Review Board Statement: Not applicable.

Informed Consent Statement: Not applicable.

Data Availability Statement: Not applicable.

Conflicts of Interest: The authors declare no conflict of interest.

References

1. Xie, Y.; Xiao, J. Research on the Development Status and Trend of High speed Railway. *High Speed Railw. Technol.* **2021**, *12*, 23–26.
2. Xiao, H.; Wu, Z.; Huang, X. Analysis on the cause of fatigue fracture of high-speed rail fastener spring bar. *Ind. Saf. Environ. Prot.* **2021**, *47*, 50–54.
3. Li, T.-T.; Bai, Y.-H.; Liu, Z.-R.; Liu, J.-F.; Zhang, G.-S.; Li, J.-L. Air quality in passenger cars of the ground railway transit system in Beijing, China. *Sci. Total Environ.* **2006**, *367*, 89–95. [CrossRef] [PubMed]
4. Liu, J.G.; Gong, G.P.; Yan, C.W. EIS study of corrosion behaviour of organic coating/Dacromet composite systems. *Electrochim. Acta* **2005**, *50*, 3320–3332.
5. Zhang, S.; Zhang, Y.; Yu, H.; Ru, J.; Lv, M. Study on zinc impregnation process and anti-corrosion performance of elastic rod. *Railw. Build.* **2021**, *61*, 122–124.
6. Hu, H.; Li, N.; Cheng, J.; Chen, L. Corrosion behavior of chromium-free dacromet coating in seawater. *J. Alloy. Compd.* **2009**, *472*, 219–224. [CrossRef]

7. Hiroaki, N. Effects of plating factors on morphology and appearance of electrogalvanized steel sheets. *Trans. Nonferrous Met. Soc. China* **2009**, *19*, 835–841.

8. Jyotheender, K.S.; Punith Kumar, M.K.; Srivastava, C. Low temperature electrogalvanization: Texture and corrosion behavior. *Appl. Surf. Sci.* **2021**, *559*, 149953. [CrossRef]

9. Kurebayashi, Y.; Ito, Y.; Yoneguchi, A. Development of new high strength spring steel and its application to automotive coil spring. *Trans. Jpn. Soc. Spring Eng.* **2000**, *2000*, 1–7. [CrossRef]

10. Qian, H.; Xu, Z.W.; Chen, S.K. Silicon carbide/enamel composite coatings for steel corrosion protection: Microstructure, thermal expansion behavior, and anti-corrosion performance. *Surf. Coat. Technol.* **2022**, *434*, 128172. [CrossRef]

11. Zhao, X.; Yi, X.; Hu, P. Discussion on the status quo and prospect of spring steel production. *China Met. Bull.* **2019**, *4*, 251–252.

12. Podgornik, B.; Leskovšek, V.; Godec, M.; Senčič, B. Microstructure refinement and its effect on properties of spring steel. *Mater. Sci. Eng. A* **2014**, *599*, 81–86. [CrossRef]

13. Georgy, L.; Anton, K.; Tatiana, N. Anti-corrosion coatings for protection of steel railway structures exposed to atmospheric environments: A review. *Constr. Build. Mater.* **2021**, *288*, 123115.

14. Komazaki, S.I.; Kobayashi, K.; Misawa, T.; Fukuzumi, T. Environmental embrittlement of automobile spring steels caused by wet–dry cyclic corrosion in sodium chloride solution. *Corros. Sci.* **2005**, *47*, 2450–2460. [CrossRef]

15. He, W.; Chen, Y.L.; Yu, W.; Su, L.; Wang, X.; Tang, D. Study on corrosion resistance of high-strength medium-carbon spring steel and its hydrogen-induced delayed fracture. *Constr. Build. Mater.* **2020**, *239*, 117815.

16. Sun, M.; Hui, W.; Zhang, D.; Dong, Y. Effect of Ni on corrosion fatigue properties of medium carbon high strength spring steel. *Spec. Steel* **2008**, *29*, 52–54.

17. Zuo, M.; Chen, Y.; Mi, Z.; Niu, G.; Wang, Y. Phase composition and transformation of corrosion products of Cr, V alloyed spring steels. *Corros. Sci. Prot. Technol.* **2019**, *31*, 475–482.

18. Zhang, C.; Han, Q.; Sun, S.; Zhang, H.; Liu, Y.; Zhou, L. Effect of Nb-V composite microalloying on corrosion resistance of 60Si2MnA spring steel. *Met. Heat Treat.* **2010**, *35*, 42–44.

19. Zhang, S.; Zhang, Y.; Yu, H.; Lv, M. Study on adhesion and antirust performance of anticorrosive coating for elastic rod by powder electrostatic spraying process. *Railw. Build.* **2020**, *60*, 138–140.

20. Wang, W.; Wang, S.; Shan, Y.; Yang, K. Study on atmospheric corrosion properties of steel spring materials for high-speed trains. *Corros. Sci. Prot. Technol.* **2010**, *22*, 511–513.

21. Song, C. Overview of the status quo of bullet bar anti-corrosion technology for high-speed railway in China. *Digit. Users* **2018**, *41*, 24–25.

22. Wu, H.T.; Han, X.T.; Zhao, W. Mechanical and electrochemical properties of UV-curable nanocellulose/urushiol epoxy acrylate anti-corrosive composite coatings. *Ind. Crops Prod.* **2022**, *181*, 114805. [CrossRef]

23. Mousavi, B.; Farvizi, M.; Rahimipour, M.R. Comparison of the hot corrosion behavior of the LZ, CSZ and LZ/CSZ composite thermal barrier coating. *Surf. Coat. Technol.* **2022**, *437*, 128324. [CrossRef]

24. Zhou, C.; Zhang, Y.; Hui, W.; Wang, L. Effect of hydrogen on ultra-high cycle fatigue properties of 60Si2CrVA spring steel. *J. Iron Steel Res.* **2013**, *25*, 45–51.

25. Xiao, G.Z.; Di, H.S. Delayed fracture resistance and mechanical properties of 30MnSi high strength steel. *J. Iron Steel Res. Int.* **2009**, *16*, 49. [CrossRef]

26. Masoud, M.; Mahdieh, S. Temperature mitigates the hydrogen embrittlement sensitivity of martensitic steels in slow strain rates. *Vacuum* **2022**, *202*, 111187.

27. Tomoki, D.; Hiroshi, S.; Kenichi, T. Enhanced Lattice Defect Formation Associated with Hydrogen and Hydrogen Embrittlement under Elastic Stress of a Tempered Martensitic Steel. *ISIJ Int.* **2012**, *52*, 198–207.

28. *ISO 5952-2019*; Steel Sheet, Hot-Rolled, of Structural Quality with Improved Atmospheric Corrosion Resistance (Annex A A.3.2). ISO: Geneva, Switzerland, 2019.

29. *ASTM G101-04*; Standard Guide for Estimating the Atmospheric Corrosion Resistance of Low Alloy Steels; Reapproved 2010. ASTM International: West Conshohocken, PA, USA, 2004.

30. Tsay, L.W.; Lu, H.F.; Chen, C. The effect of grain size and aging on hydrogen embrittlement of a maraging steel. *Corros. Sci.* **2008**, *50*, 2506. [CrossRef]

31. Gan, L.; Huang, F.; Zhao, X.; Liu, J.; Cheng, Y.F. Hydrogen trapping and hydrogen induced cracking of welded X100 pipeline steel in H2S environments. *Int. J. Hydrog. Energy* **2018**, *43*, 2293–2306. [CrossRef]

32. Zhao, J.W.; Jiang, Z.Y.; Lee, C.S. Effects of tungsten on the hydrogen embrittlement behavior of microalloyed steels. *Corros. Sci.* **2014**, *21*, 32–35.

33. McCarty, E.D.; Wetzel, D.; Kloberdanz, S. Hydrogen embrittlement in automotive fastener applications. *SAE Trans.* **1996**, *105*, 355–383.

34. Liu, Q.; Venezuela, J.; Zhang, M.; Zhou, Q.; Atrens, A. Hydrogen trapping in some advanced high strength steels. *Corros. Sci.* **2016**, *111*, 770–785. [CrossRef]

35. Basukumar, H.K.; Arun, K.V. Tensile behavior of pre-stress corroded and post hydrogen embrittled spring steel. *Mater. Today Proc.* **2022**, *49*, 2000–2006. [CrossRef]

36. Liu, Q.; Atrens, A. Reversible hydrogen trapping in a 3.5NiCrMoV medium strength steel. *Corros. Sci.* **2015**, *96*, 112–120. [CrossRef]

37. Gibala, D.D.S. *Hydrogen in Metals*; AIME: Mountain View, CA, USA, 1981; p. 113.

38. Ke, S. Study on Hydrogen Embrittlement Sensitivity and Hydrogen Permeation Behavior of DP600 Steel. Master's Thesis, Wuhan University of Science and Technology, Wuhan, China, 2018.

39. Zhao, H.Y.; Wang, P.; Li, J.X. Effect of vanadium content on hydrogen embrittlement of 1400 MPa grade high strength bolt steels. *Int. J. Hydrog. Energy* **2021**, *46*, 34983–34997. [CrossRef]

40. Jeffrey, V.; Fang, Y.L.; Li, L.; Sonia, J. Hydrogen embrittlement of an automotive 1700 MPa martensitic advanced high-strength steel. *Corros. Sci.* **2020**, *171*, 108726.

41. Venezuela, J.; Zhou, Q.; Liu, Q.; Li, H.; Zhang, M.; Dargusch, M.S.; Atrens, A. The influence of microstructure on the hydrogen embrittlement susceptibility of martensitic advanced high strength steels. *Mater. Today Commun.* **2018**, *17*, 1–14. [CrossRef]

42. Wang, X.; Chen, Y.; Xu, L. Effect of alloying elements Mn, Cr, V on the tempering structure and mechanical properties of medium carbon spring steel. *Hot Work. Process* **2016**, *45*, 183–186.

43. Toyoda, S.; Ishiguro, Y.; Kawabata, Y.; Sakata, K.; Sato, A.; Sakai, J. Effect of Cu Addition on Delayed Fracture Resistance of Low Carbon Steel for 1470 MPa Grade Electric Resistance Welded Tube. *ISIJ Int.* **2008**, *48*, 640–648. [CrossRef]

44. Furuya, Y.; Hirukawa, H.; Hayakawa, M. Gigacycle Fatigue Properties of Hydrogen-Charged JIS-SCM440 Low-Alloy Steel Under Ultrasonic Fatigue Testing. *Metall. Mater. Trans. A* **2010**, *41*, 2248–2256. [CrossRef]

45. Diaz, I.; Cano, H.; De la Fuente, D.; Chico, B.; Vega, J.M.; Morcillo, M. Atmospheric corrosion of Ni-advanced weathering steels in marine atmospheres of moderate salinity. *Corros. Sci.* **2013**, *76*, 348–360. [CrossRef]

46. Kamimura, T.; Stratmann, M. The influence of chromium on the atmospheric corrosion of steel. *Corros. Sci.* **2001**, *43*, 429–447. [CrossRef]

47. Liu, Y.; Li, S.; Li, Y.; Yang, Z. Factors influencing the GBF size of high strength steels in the very high cycle fatigue regime. *Mater. Sci. Eng.* **2011**, *528*, 935–942. [CrossRef]

48. Chatzidouros, E.V.; Papazoglou, V.J.; Pantclis, D.I. Hydrogen effect on a low carbon ferritic-bainitic pipeline steel. *Int. J. Hydrog. Energy* **2014**, *39*, 18498–18505. [CrossRef]

49. Toshiaki, O.; Tomohiro, K. Enhancement of electric conductivity of the rust layer by adso-rption of water. *Corros. Sci.* **2005**, *47*, 2571–2577.

50. Song, X.; Wang, K.; Zhou, L.; Chen, Y.; Ren, K.; Wang, J.; Zhang, C. Multi-factor mining and corrosion rate prediction model construction of carbon steel under dynamic atmospheric corrosion environment. *Eng. Fail. Anal.* **2022**, *134*, 105987. [CrossRef]

51. Ishikawa, T.; Takeuchi, K.; Kandori, K.; Nakayama, T. Transformation of γ-FeOOH to α-FeOOH in acidic solutions containing metal ions. *Colloids Surf. A Physicochem. Eng. Asp.* **2005**, *266*, 155–159. [CrossRef]

52. Liu, H.; Cao, F.; Song, G.-L.; Zheng, D.; Shi, Z.; Dargusch, M.S.; Atrens, A. Review of the atmospheric corrosion of magnesium alloys. *J. Mater. Sci. Technol.* **2019**, *35*, 2003–2016. [CrossRef]

53. Zhang, H.; Zhang, J.; Wu, B.; Hu, X.; Pan, H.; Yan, J. Effect of alloying elements on atmospheric corrosion resistance of high-strength weathering steel. *J. Anhui Univ. Technol. Nat. Sci. Ed.* **2018**, *35*, 209–215.

54. Hao, L.; Zhang, S.; Dong, J.; Ke, W. Evolution of atmospheric corrosion of MnCuP weathering steel in a simulated coastal-industrial atmosphere. *Corros. Sci.* **2012**, *59*, 270–276. [CrossRef]

55. Wang, Z.; Liu, J.; Wu, L.; Han, R.; Sun, Y. Study of the corrosion behavior of weathering steels in atmospheric environments. *Corros. Sci.* **2013**, *67*, 1–10. [CrossRef]

56. Han, S. Study on Hydrogen Induced Delayed Fracture Behavior of Several High Strength Fastener Steels. Master's Thesis, Kunming University of Science and Technology, Kunming, China, 2014.

57. Zhang, H. Effect of Nb and Ni on the Delayed Fracture Behavior of High Strength Bolt Steel. Master's Thesis, Beijing Jiaotong University, Beijing, China, 2016.

58. Si, Y.; Tang, Y.; Zhou, X.; Li, K.; Ma, Y.; Ma, M. Research Progress of Microalloy Elements on Hydrogen-Induced Delayed Cracking in High Strength Martensitie Steels. *Automob. Technol. Mater.* **2022**, *6*, 16–26.

59. Shin, J.H.; Kong, B.S.; Eom, H.J.; Jang, C.; Do, H.; Jang, D. Dynamic evolution of nanosized NbC precipitates in austenite matrix during deformation and its contribution to strengthening. *Mater. Sci. Eng. A* **2021**, *806*, 140816. [CrossRef]

60. Shi, R.; Ma, Y.; Wang, Z.; Gao, L.; Yang, X.-S.; Qiao, L.; Pang, X. Atomic-scale investigation of deep hydrogen trapping in NbC/αFe semi-coherent interfaces. *Acta Mater.* **2020**, *200*, 686–698. [CrossRef]